Electronic Supplementary Material (ESI) for Biomaterials Science.

Supporting Information

Tumor Microenvironment-Activated Multi-Functional Nanodrug with Size-Enlargement for Enhanced Cancer Phototheranostics

Hongtao Chen, Bingcheng Zhou, Xian Zheng, Jie Wei, Chendong Ji*, Meizhen Yin*.

Additional Schemes and Figures

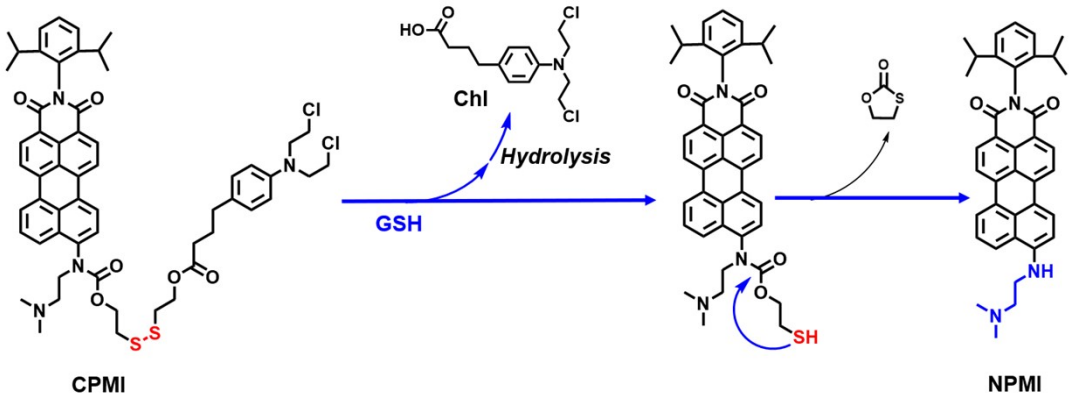

Scheme S1 Glutathione (GSH)-induced cascade reactions of prodrug CPMI to release NPMI and chlorambucil (Chl).

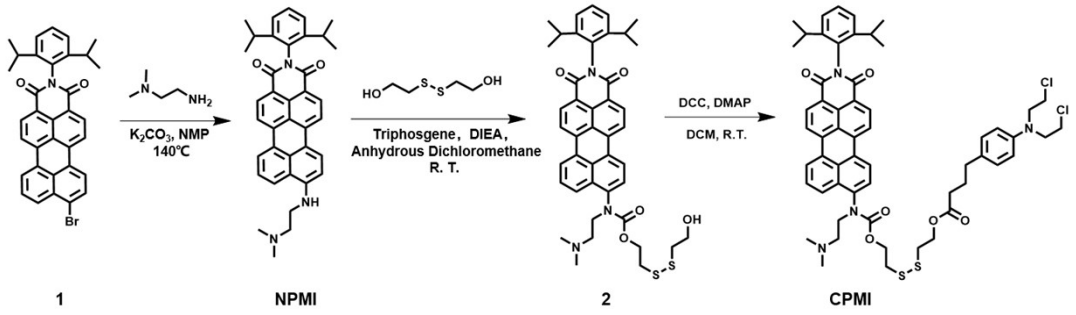

Scheme S2 Synthesis route for compounds NPMI and CPMI.

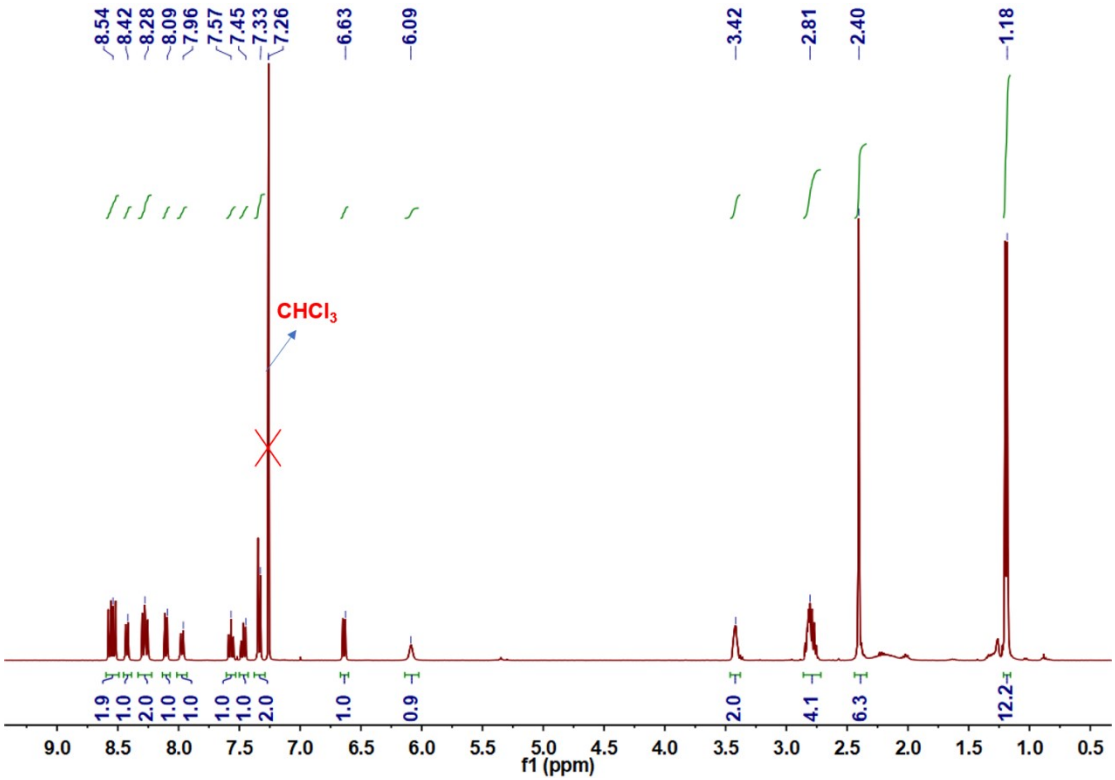

Fig. S1 ^{1}H NMR spectrum of NPMI in $CDCl_3$.

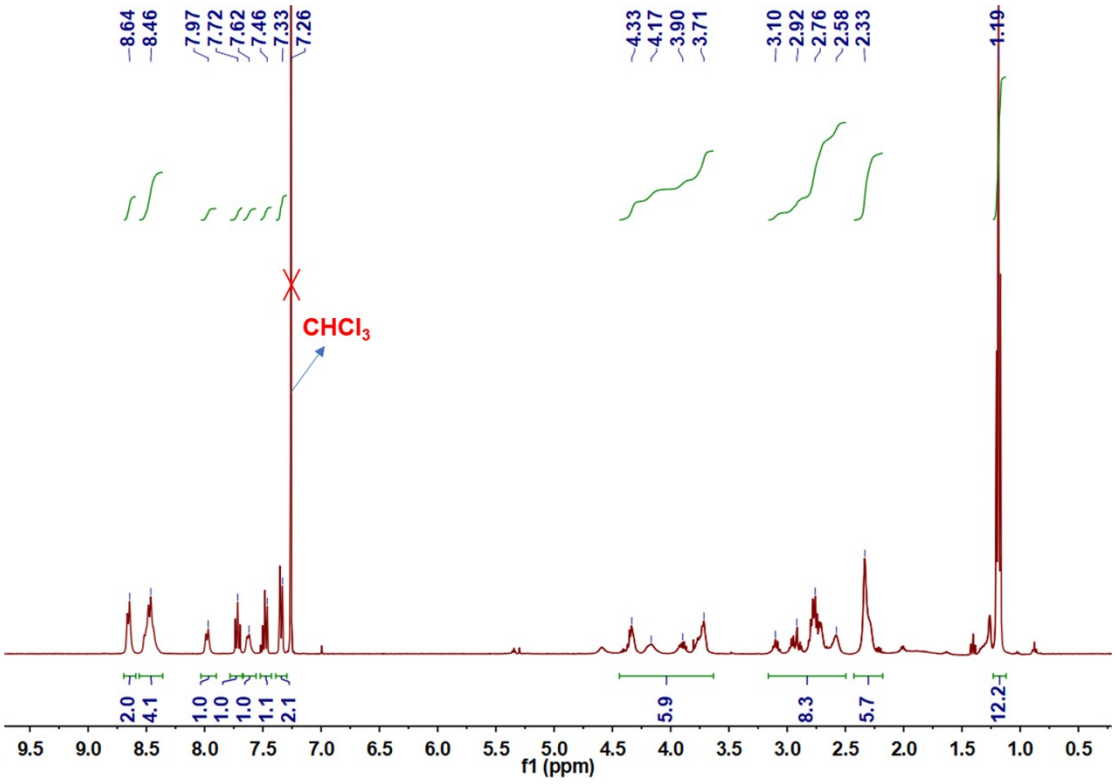

Fig. S2 ^{1}H NMR spectrum of Compound 2 in $CDCl_3$.

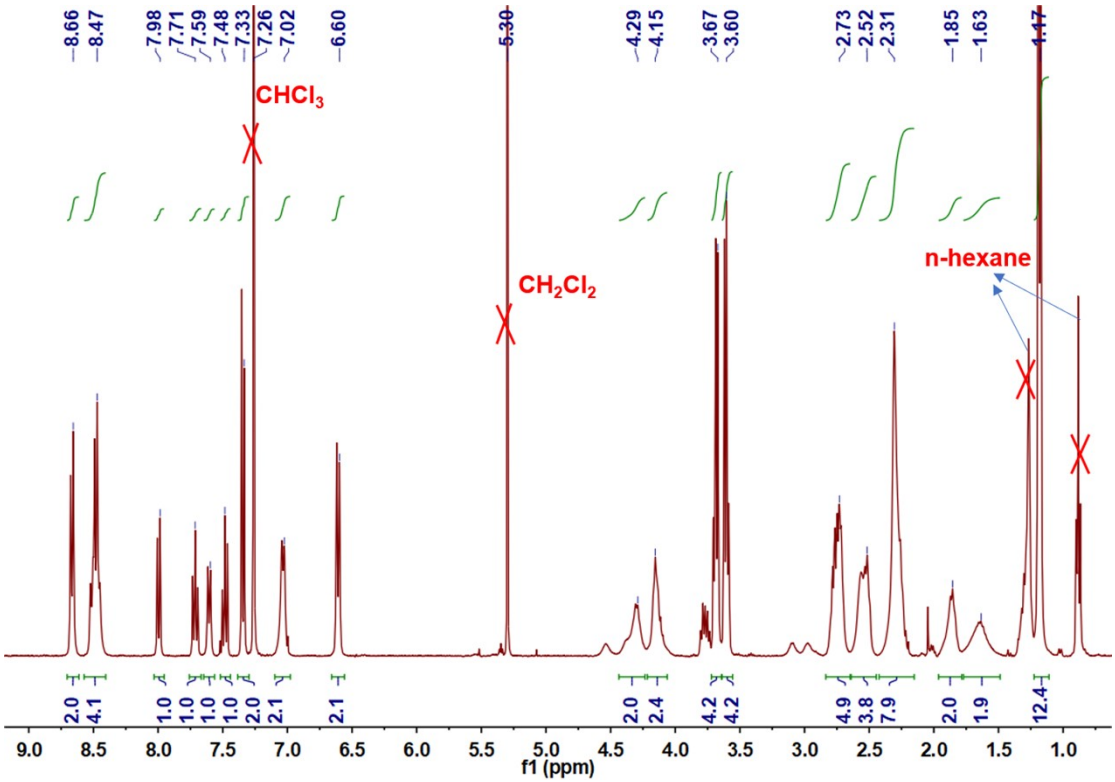

Fig. S3 ^{1}H NMR spectrum of CPMI in $CDCl_3$.

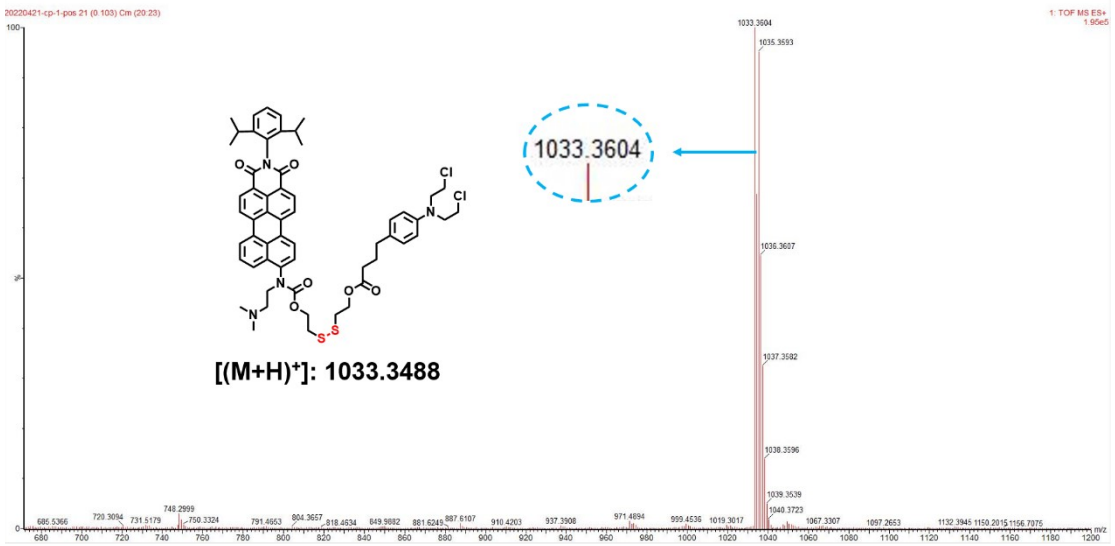

Fig. S4 Mass spectrum of CPMI.

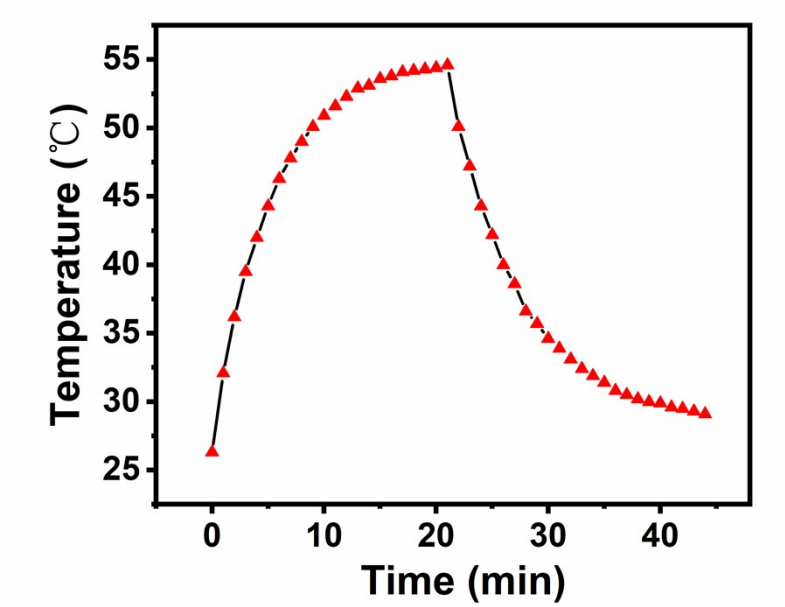

Fig. S5 Temperature increases of NPMI aqueous solution (with 1% DMSO) under laser irradiation (660 nm, 1.0 W/cm^2). The laser was removed when the temperature had reached maximum.

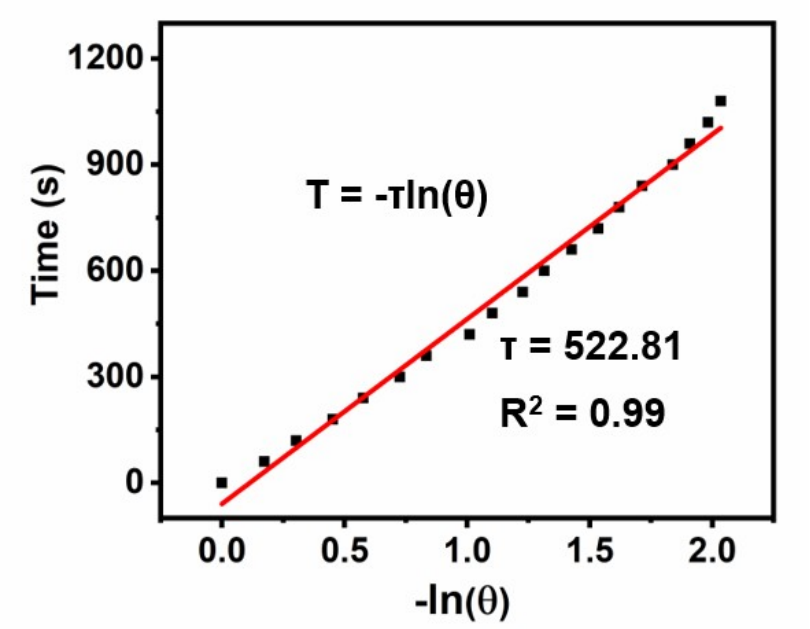

Fig. S6 The relationship between cooling time t and ln(θ) in the photothermal conversion efficiency (PCE) measurement of NPMI.[1] The time constant τ was calculated as 522.81.

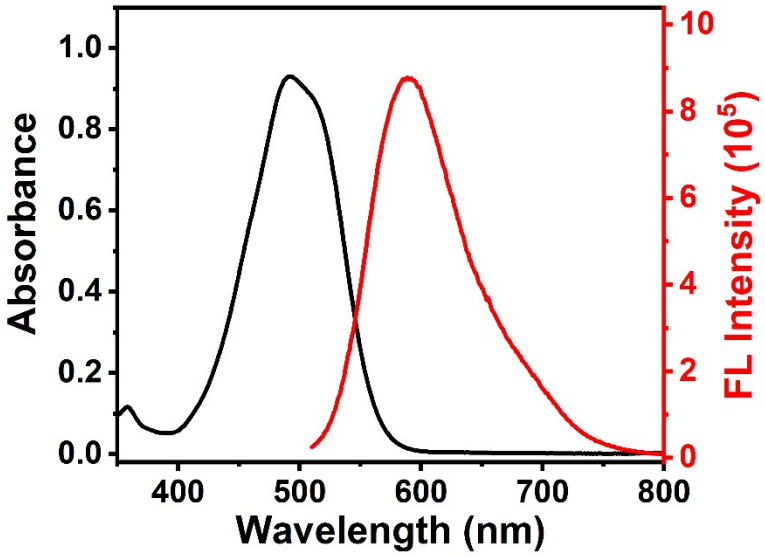

Fig. S7 UV-Vis-NIR absorption and fluorescence spectra (λ_{ex} = 494 nm) of CPMI NP in deionized water (Concentration: 10 μM).

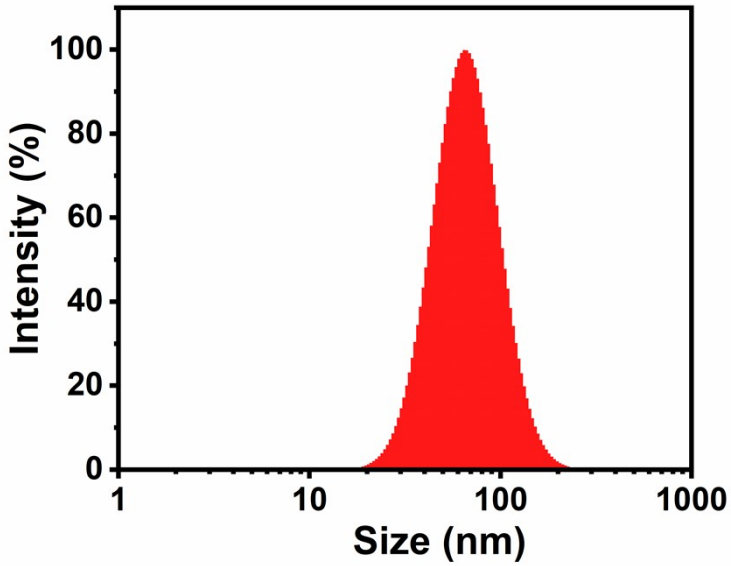

Fig. S8 Size distribution of NPMI NP (20 μM) obtained by dynamic laser scattering (DLS) at 25 °C. The average particle size is 66 nm.

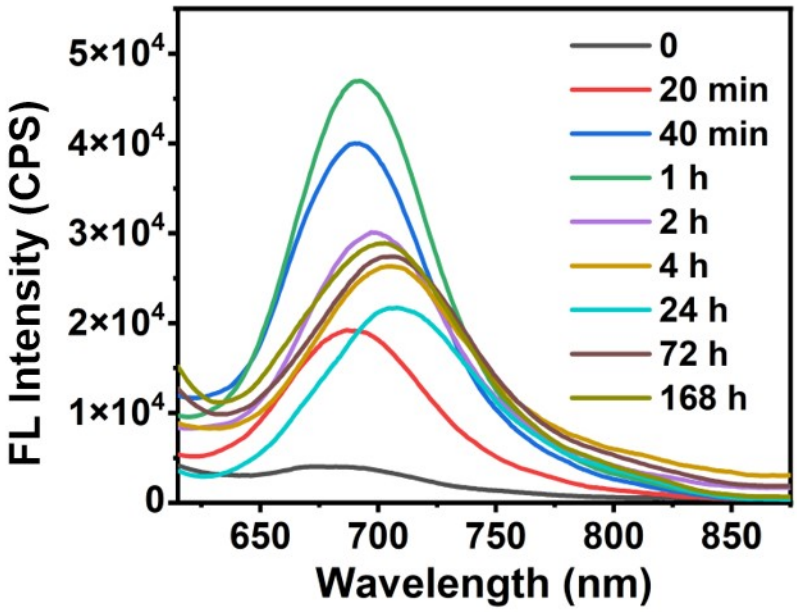

Fig. S9 Time-dependent fluorescence spectra of CPMI NP (10 μM) after 10 mM GSH addition at 37 °C.

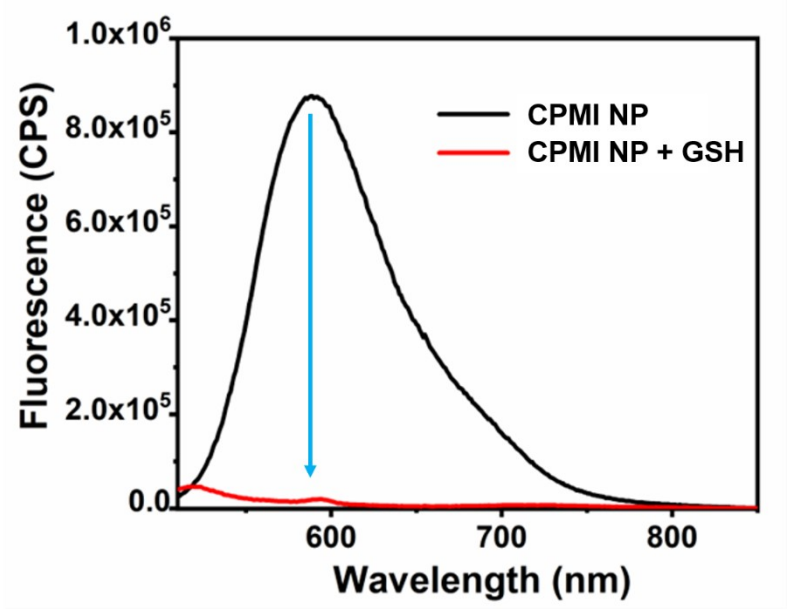

Fig. S10 Fluorescence spectra of CPMI NP (10 μM) before and after GSH response (λ_{ex} = 490 nm).

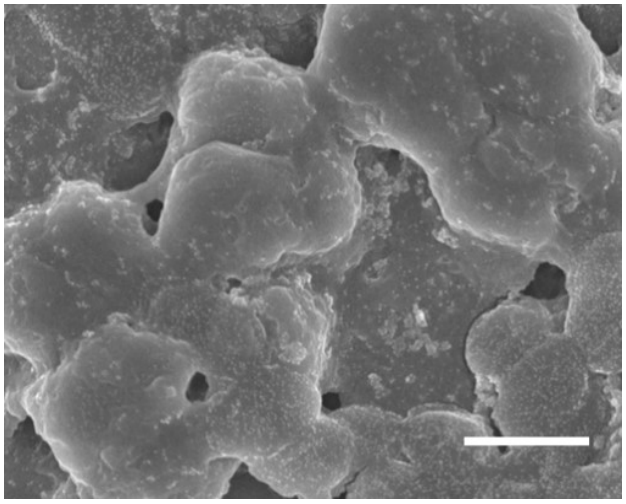

Fig. S11 Scanning electron microscopy (SEM) image of the blue precipitate formed by CPMI NP after GSH response. Scale bar: 1 μm.

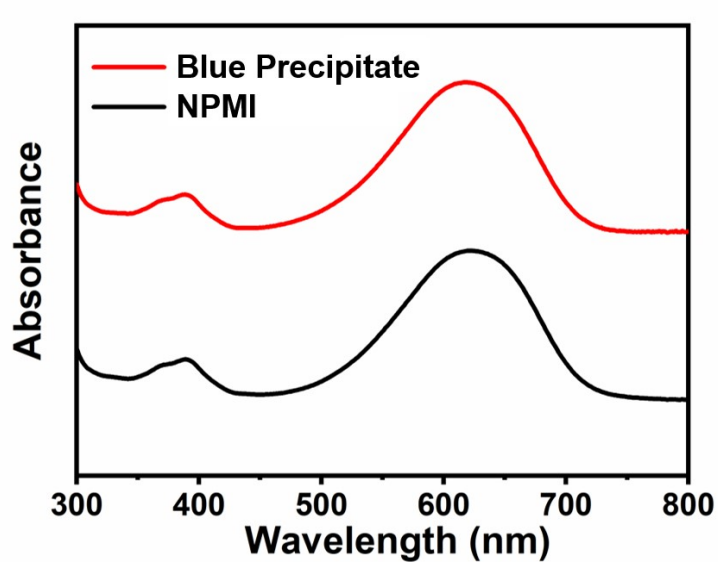

Fig. S12 UV-Vis-NIR absorption spectra of the precipitate and NPMI in dichloromethane.

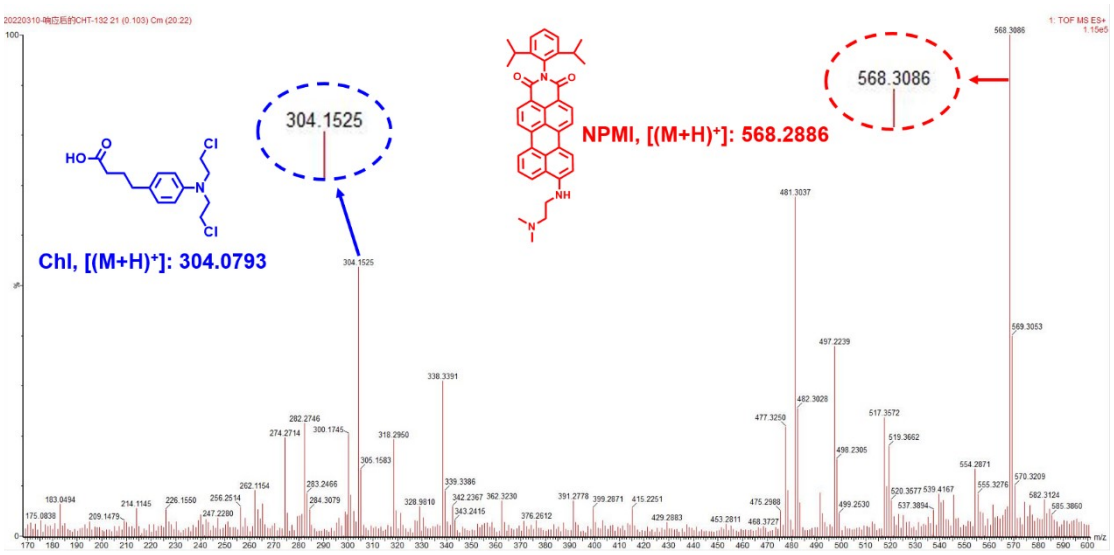

Fig. S13 Mass spectrum of the blue precipitate formed by CPMI NP after GSH response. The molecular weight 568.3086 is agreeable with the theoretical value of NPMI (568.2886). The molecular weight 304.1525 is agreeable with the theoretical value of Chl (304.0793).

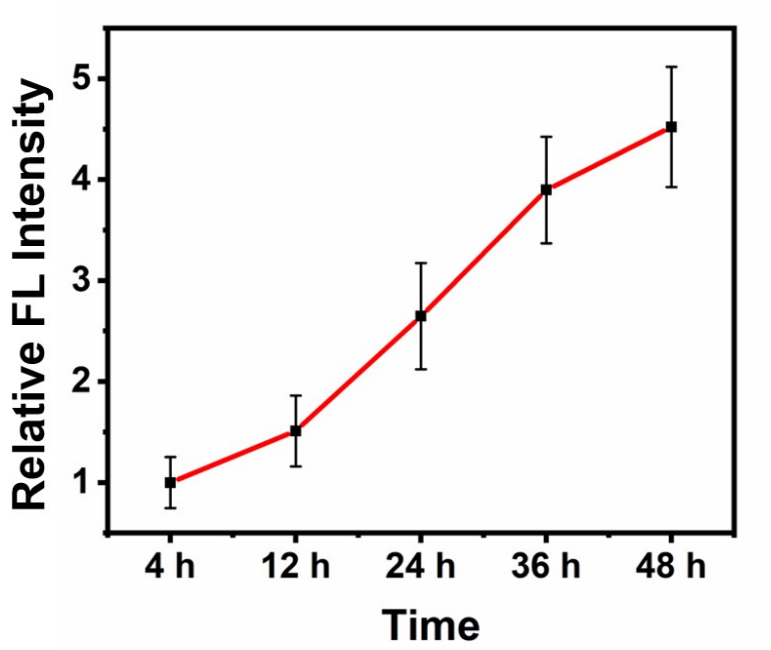

Fig. S14 The time-dependent fluorescence intensities of 4T1 cells after cultivation with CPMI NP (20 μM) for 4 h.

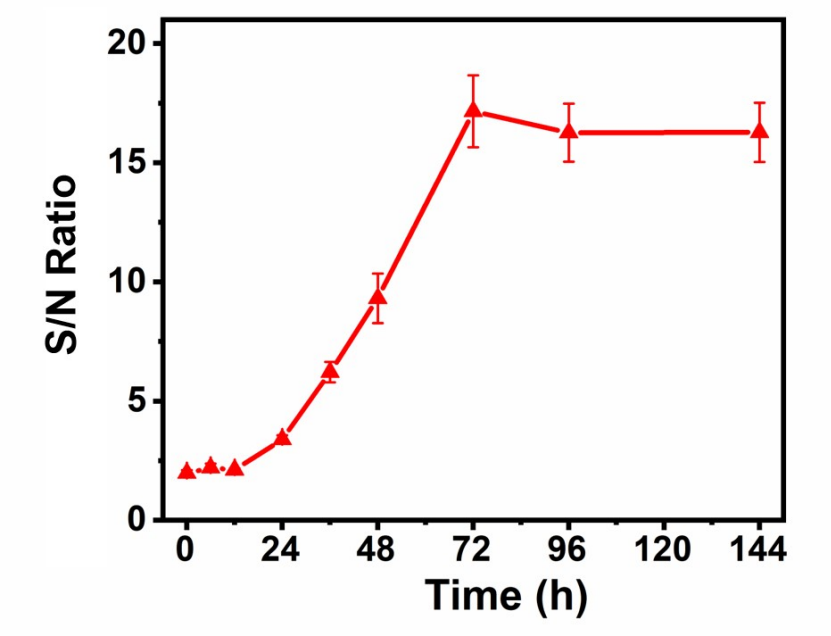

Fig. S15 The signal-to-noise (S/N) ratio changes at tumor site of *in vivo* fluorescence imaging.

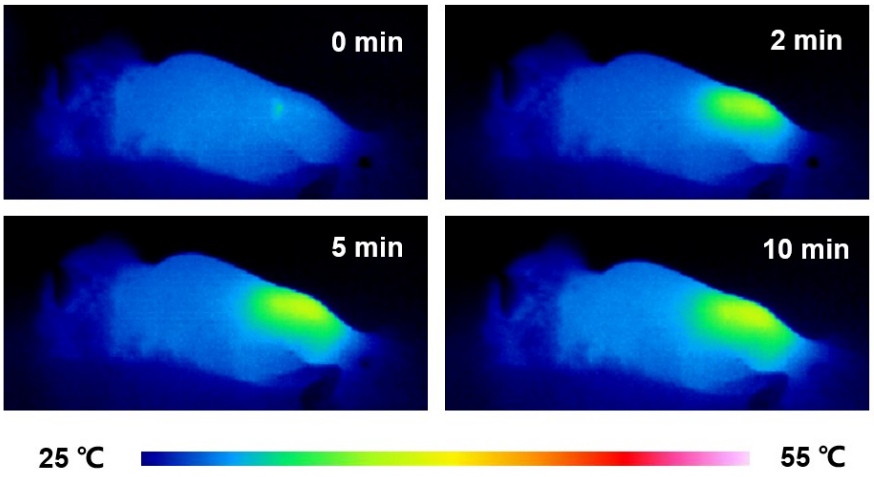

Fig. S16 Infrared thermal images of the mice with the subcutaneous tissue being exposed to the laser light (660 nm, 0.5 W/cm^2) after CPMI NP administration.

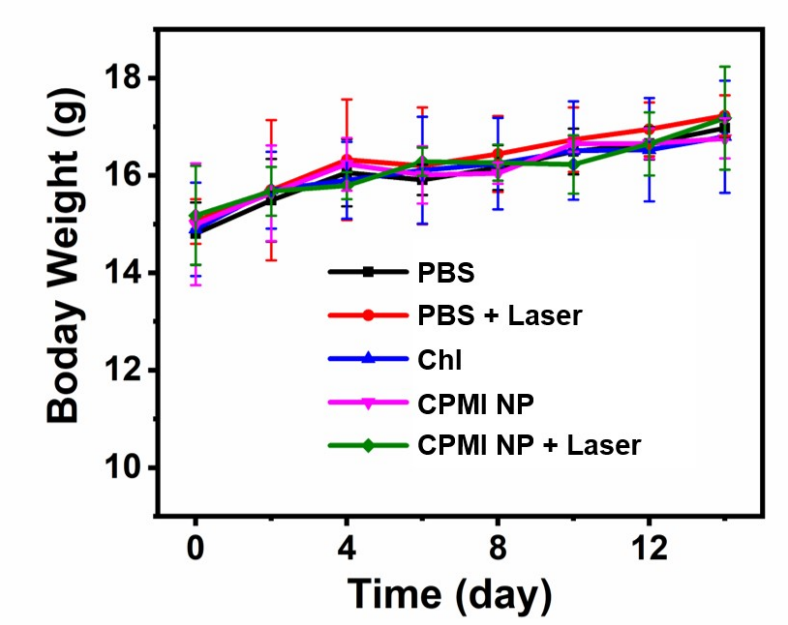

Fig. S17 Average body weights of mice in each group during treatments.

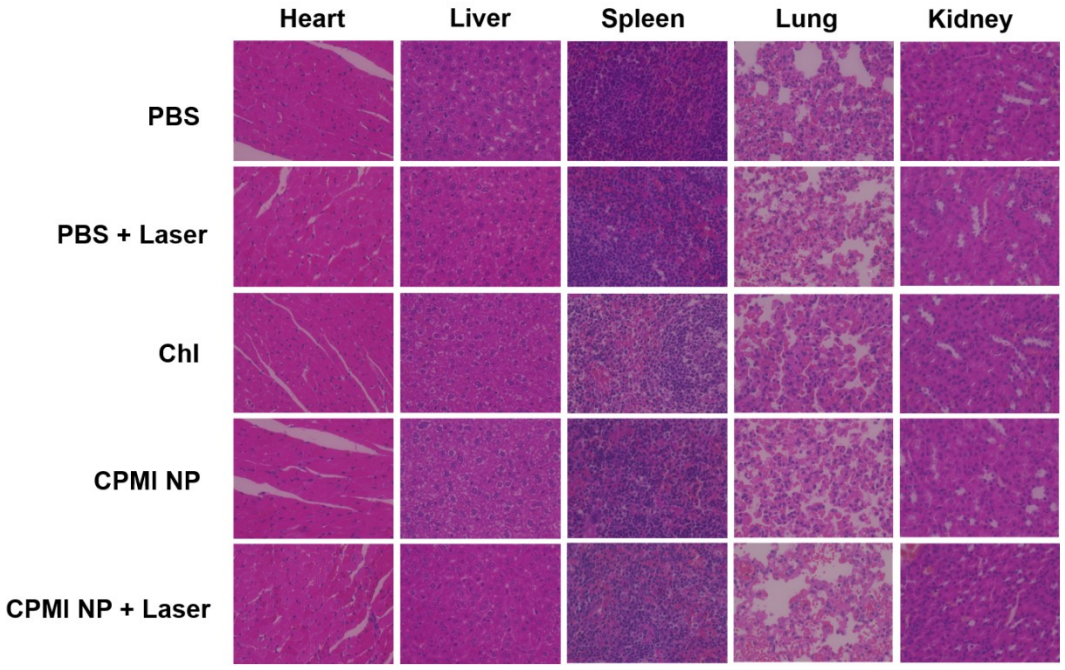

Fig. S18 Histological analysis of the major organs (heart, liver, spleen, lung, and kidney) collected from mice in the different groups after treatment with H&E staining.

Reference:

1. S. Zhang, W. Guo, J. Wei, C. Li, X. J. Liang, M. Yin, *ACS Nano*, 2017, **11**, 3797-3805.